AD A124 477 FACTORS CONTROLLING WELD METAL CHEMISTRY(U) SELSKAPET FOR INDUSTRIELL OG TEKNISK FORSKNING VED NORGES TEKNISKE HOEGSKOLE TRONDHEIM O GRONG ET AL. AUG 82 1/1

UNCLASSIFIED SINTEF-341094 DAJA37-81-C-0309 F/G 13/8 NL

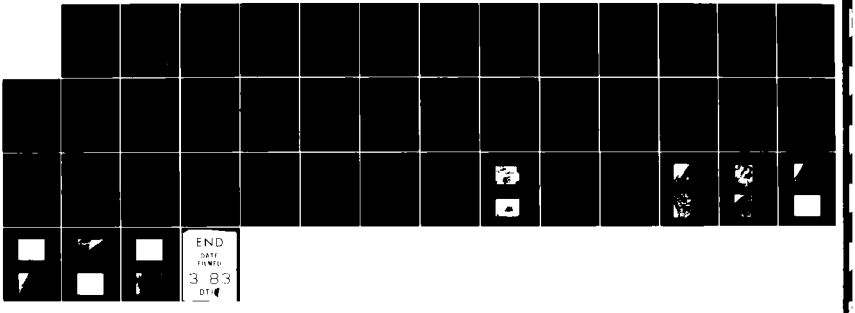

END
DATE FILMED
3 83
DTIC

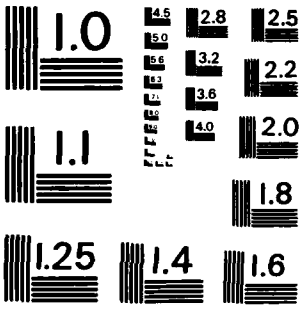

MICROCOPY RESOLUTION TEST CHART
NATIONAL BUREAU OF STANDARDS - 1963 - A

(12)

AD

FACTORS CONTROLLING WELD METAL CHEMISTRY

Final Technical Report

by

Ø. Grong and N. Christensen

August, 1982

United States Army

EUROPEAN RESEARCH OFFICE OF THE U.S. ARMY

London England

CONTRACT NUMBER ..... DAJA 37-81-C-0309

SINTEF - The Foundation of Scientific and Industrial Research
at the Norwegian Institute of Technology

UNCLASSIFIED

SECURITY CLASSIFICATION OF THIS PAGE (When Data Entered)

REPORT DOCUMENTATION PAGE	READ INSTRUCTIONS BEFORE COMPLETING FORM
1. REPORT NUMBER	2. GOVT ACCESSION NO. AD-A124 477 / 3. RECIPIENT'S CATALOG NUMBER
4. TITLE (and Subtitle) Factors Controlling Weld Metal Chemistry	5. TYPE OF REPORT & PERIOD COVERED Final Technical Report June 1982
	6. PERFORMING ORG. REPORT NUMBER SINTEF - 341094
7. AUTHOR(s) Ö. Grong and N. Christensen	8. CONTRACT OR GRANT NUMBER(s) DAJA37-81-C-0309
9. PERFORMING ORGANIZATION NAME AND ADDRESS SINTEF N-7034 Trondheim - NTH Norway	10. PROGRAM ELEMENT, PROJECT, TASK AREA & WORK UNIT NUMBERS 1T161102BH57-04
11. CONTROLLING OFFICE NAME AND ADDRESS USARDSG-UK Box 65 FPO New York 09510	12. REPORT DATE June 1982
	13. NUMBER OF PAGES 30
14. MONITORING AGENCY NAME & ADDRESS(if different from Controlling Office)	15. SECURITY CLASS. (of this report) Unclassified
	15a. DECLASSIFICATION/DOWNGRADING SCHEDULE

16. DISTRIBUTION STATEMENT (of this Report)

Approved for public release; Distribution unlimited

17. DISTRIBUTION STATEMENT (of the abstract entered in Block 20, if different from Report)

18. SUPPLEMENTARY NOTES

19. KEY WORDS (Continue on reverse side if necessary and identify by block number)

GMA welding
Melt spinning quench
Electrode tip reactions
Arc column reactions
Weld pool reactions

20. ABSTRACT (Continue on reverse side if necessary and identify by block number)

This work is intended to elucidate the kind and extent of chemical interaction in the four main steps of the GMA process: (1) electrode tip, (2) arc column, (3) hot part of weld pool, and (4) cooling part of weld pool. Identification of reaction sites has been made by local sampling and by suppressing the weld pool stage in welding onto a fast spinning cold copper wheel. Each stage may be briefly described as follows:

(1) Oxidation of carbon and alloying elements.

cont.

DD FORM 1 JAN 73 1473 EDITION OF 1 NOV 65 IS OBSOLETE S/N 0102-LF-014-6601

UNCLASSIFIED

SECURITY CLASSIFICATION OF THIS PAGE (When Data Entered)

Continued item (20)

(2) Re-dissolution of silicates formed in stage (1)
Evaporation of Fe and Mn, preventing further interaction.
(3) Absorption of oxygen, of the order of four times the analytical content of chilled metal or ten times that of multi-layer deposit.
(4) Precipitation of slag particles, and separation of a main fraction of the micro-slag.

Implications of this sequence of reactions for design of filler metal and choice of operational conditions are briefly discussed.

SUMMARY

The melt spinning technique, originally being developed for production of amorphous alloy ribbons has been applied in studies of high temperature reactions occuring in the MIG arc plasma. In this case the arc is maintained between a continously melting electrode and a water-cooled, fast rotating copper wheel (spinner). The liquid metal droplets released from the electrode tip are rapidly cooled on the spinner surface. The speed of quenching attained is sufficient to freeze the metal composition established at high temperature. By analytical comparison of collected electrode tip droplets and multi-run weldments, taking the oxygen potential in the shielding gas as the only variable, the reaction pattern in MIG welding at different stages of the process may be schematically presented as follows:

Shielding gas interaction	Metal reaction	Approximate temperature level
	Electrode wire	
	↓	
	Tip droplet	
	SiO_2-MnO-Feo slag formed	
Oxygen absorbed →	Carbon oxidized	1600°C
	Some Si lost as SiO gas	
	↓	
	Falling droplets	
Oxygen pick-up restricted by Mn and Fe evaporation →	Silicate slag dissolves	
	Mn and Fe evaporate	2400°C
	↓	
	Hot zone of the weld pool	
	Increased oxygen pick-up	
Oxygen extensively absorbed →	Unfavourable nucelation conditions largely prevent C, Si and Mn oxidation	2000°C
	↓	
	Cooling part of the weld pool	
	Si and Mn deoxidation reactions	
Oxygen pick-up unfavourable →	High residual oxygen due to uncomplete oxide phase separation	<1700°C
	↓	
	Final weld metal composition	

TABLE OF CONTENTS

1. INTRODUCTION

The present investigation is concerned with a fundamental study of mechanisms controlling weld metal chemistry. It is intended to test experimentally a simple model for predicting, or at least estimating the extent of chemical interaction of liquid weld metal with its surroundings (arc atmosphere, slag). The model referred to is based on the assumption of:

- A high temperature stage where the chemical reactions are approaching a state of local pseudo-equilibrium.

- A cooling stage where the concentrations established during the first stage tend to re-adjust by precipitation of new phases.

A temperature range from 2000-2400°C is assumed for the high temperature stage, where chemical interaction occurs at the phase boundary between arc atmosphere and weld metal. Included in the high temperature stage are also reactions occurring in the hot part of the weld pool. The second stage starts when the arc has passed. The changes taking place in the cooler part of the pool are characterized by deoxidation reactions, i.e., by precipitation of non-metallic inclusions in the pool followed by a more or less complete separation of the dispersed particles in the form of a macroscopic slag phase.

Although chemical reactions in arc welding are often referred to in the literature, it seems not yet clarified whether the controlling reactions are located in the weld pool or in the arc plasma. Uncertainties of this kind arise from difficulties in sampling the high temperature stage. High transient concentrations of carbon and oxygen may exist in the liquid metal at elevated temperatures as a result of interaction with the arc atmosphere or, in the case of a macroscopic slag phase, from dissolution of oxygen, silicon and manganese. On slow cooling down to the solidification temperature, this will lead to spontaneous reaction and losses of dissolved elements due to CO gas formation and iron-manganese silicate slag precipitation. However, these reactions may not proceed to equilibrium.

For this reason studies of high temperature reactions will be entirely dependent on the experimental method applied, i.e., on the possibilities of quenching-in the concentrations established in the metal phase during the high temperature stage. From a literature survey it appears that several attempts have been made to develop an adequate technique, but none of the reported methods seem so far to have made a separate study of the two different stages possible.

2. DEVELOPMENT OF EQUIPMENT

In order to study the high temperature reactions in arc welding, a new experimental technique has been worked out, based on the principles of metal spinning originally being developed by Maringer /1/ for production of amorphous alloy ribbons. In this case the arc is maintained between a continuously melting electrode and a water-cooled, fast rotating copper wheel (spinner). The liquid metal droplets released from the electrode tip are rapidly cooled on the spinner surface.

2.1. Testing procedure

So far, only MIG welding has been examined. In this case a conventional MIG welding power source and wire feed system was tested in combination with a copper spinner. The results obtained appeared promising. The arc stability was good and seemed unaffected by increasing welding speed in the range from 7 to 11 m/s*). At the same time the droplet transfer was steady and fume generation small.

Chilled metal was collected in the form of strips (1-2mm wide of an average thickness 50-100μm), which were continuously detached from the wheel surface. The characteristic shape of the metal indicates a very rapid solidification, estimated to be in the order of 10^5 °C/s. This is not far from the reported values of ordinary metal spinning, stated to be in the range of 10^5-10^6 °C/s. Consequently, the dissipation of the arc power on the wheel surface appears not to have effected the cooling rate significantly.

An important factor in producing uniform strips without any formation of a macroscopic oxide skin, seems to be the cleanliness of the spinner surface. In the case of an oxidizing arc atmosphere, the wheel surface was covered by black copper oxide which reduced the cooling rate and caused a delayed solidification on the wheel. However, the use of a rotating steel brush effectively removed most of the copper oxide coating, resulting in a slightly roughened wheel surface. According to Huang and Fiedler /4/ a steel brush applied in this way gives the advantage of an increased interfacial heat transfer due to the cleaner surface conditions and the greater metal/wheel contact area. The conditions for obtaining uniform metal strips without any oxide formation were further improved by mechanical weaving of the electrode and by an efficient water-cooling of the copper spinner. The arc power dissipation on the wheel did not cause any wear or

*) According to Guile and Hitchcock /2,3/, it is possible to have a stable arc between an electrode and a water-cooled copper cathode at velocities up to about 110-130m/s.

damage of surface in the case of an oscillating electrode.

2.2. Final equipment design

Based on the experience gaind in these preliminary experiments and on fruitful discussions with staff members of the melt spinning group at SINTEF, the final equipment was constructed as shown in Fig. A.1 (Appendix A).

In this case the water-cooled copper wheel (150mm dia. and 50mm wide) is placed inside a closed chamber (volume 21 litre), which makes it possible to perform welding in a controlled gas atmosphere. On the front side, plexi-glass is used as a cover window, permitting inspection of the welding process. In order to minimize instability in the wire feed system, the wire feed unit is placed immediately above the chamber. A special design of the electrode holder was worked out to enable mechanical weaving inside the closed chamber, using a Z-shaped wire guide oscillated by means of an electrically controlled pneumatic cylinder. To keep the copper wheel free from contamination, a 100mm dia. steel brush has been provided, revolving at the same speed as the copper spinner counterwise to the casting direction of the wheel. On the opposite side, a teflon scraper is mounted to faciliate ribbon detachment from the wheel surface. The spinner is driven by a 1 hp D.C. motor, giving stable conditions in spite of variations in the load.

Controlled mixing of shielding gases is done by use of 2 flow-meters, one for oxygen and one for argon or CO_2 respectively. This allows variations in the gas composition over a wide range.

The copper spinner may easily be removed and replaced by the equipment used for multi-run weld metal deposition on plate (Fig. A.2). This consists of a moving table, driven in the horizontal direction by means of a spindle. Mild steel coupons (135mm x 95mm x 15mm) are attached to the top of the table. Bead deposition is normally done at a welding speed of 2-5mm/s.

3. EXPERIMENTAL PROCEDURE

Welding runs have been performed in pure argon as well as in Ar-O_2 mixtures containing 2; 5; 7.5; 10; 15 and 20 vol% oxygen. For these experiments a 0.8mm copper-coated wire (OK 12.51)*) intended for CO_2 welding was selected. The chemical composition of electrode wire is given in Table B.3 (Appendix B).

---

*) Delivered by Messrs. ESAB

The average amperage and arc voltage employed were in the range of 90-100A and 24-26V respectively, corresponding to a wire feed rate of approximately 750 cm/min (electrode +). The shielding gas flow was kept constant during all experiments, equal to 20 litre/min. For the purpose of comparison, additional runs were made in pure CO_2 under identical welding conditions.

3.1. Weld metal deposition against the copper wheel

Welding against the copper wheel was done at an average pheriphery speed of 10m/s. This appeared to be close to an optimal speed in order to obtain uniform metal strips under the conditions employed. To avoid formation of a stationary liquid metal puddle on the wheel surface, the amperage had to be kept below ~ 100A. The phenomenon of puddle formation is well known from ordinary spinning of amorphous metals, where it plays an important role in the casting of uniform ribbons. In our case, however, this was disadvantageous due to the risk of additional oxygen pick-up in the liquid metal before solidification. Weaving of the electrode at an amplitude of ±20mm reduced the tendency to puddle formation at the same time as the cooling conditions were improved. Before deposition, the welding chamber was flushed with gas of equal composition as that used in the welding experiments, so as to avoid uncontrolled gas infiltration in the arc plasma as a result of turbulence set up by the rotating wheel.

When welding in atmospheres of pure argon, argon containing small amounts of oxygen, and in pure CO_2, the chilled metal formed had a bright surface luster, indicating the abscence of surface oxidation. On the other hand at increasing oxygen content in the shielding gas, some oxidation took place on the exposed solid strip surface. The bottom side, however, was unaffected. It is believed that the surface discoloration is due to secondary oxidation in the solid state, and not a result of slag precipitation in the liquid state. This is shown by chemical analysis of the chilled metal, as will be discussed later in presentation and interpretation of the experimental data.

Chilled metal was collected for chemical and metallographic examination. Chemical analyses of the carbon, oxygen, silicon and manganese contents are given in Table B.1 (Appendix B). Prior to oxygen determination, the metal was cleaned in a weak solution of HCl and subsequently washed in water and alcohol before drying in heated air. This precaution is believed to be important due to the large surface to volume ratio of chilled metal.

3.2. Additional work

In order to assess where the controlling reactions are taking place, analyses of chilled metal have been compared with multi-run weld metal deposit*). Bead deposition was done at a speed of 3mm/s under welding conditions identical to those used in deposition onto the copper wheel. Multi-layer weldments made under CO_2 or in argon containing 10 per cent or more oxygen, further allowed sampling of the thin slag layer formed on the top of the bead. Chemical analyses of multi-run weld metal deposit as well as of collected slag are given in Table B.1 (Appendix B). For purposes of comparison, electrode tip droplets were collected for chemical and metallographic examination. Measurements of the carbon content are included in Table B.1. Corresponding determination of oxygen, silicon and manganese has not been made, because the presence of slag on the tip droplets would make an interpretation of such data rather difficult. As supplementary information, top beads were deposited under Ar+20%O_2 and CO_2 onto multi-layer weldments, to which additions of carbon, silicon and manganese had been made in the form of implanted capsules. Five milimeter spacing was used between each capsule. The results of chemical analysis are given in Table B.2.

Moreover, metallographic examination of chilled metal and electrode tip droplets has been performed, both by means of optical and scanning electron microscope techniques. These results are presented in Section 4.2 and 4.6 respectively.

3.3. Methods of analysis

All determination of carbon, silicon and manganese have been done at SINTEF: carbon by combustion in oxygen, silicon gravimetric and manganese by atomic absorption. Check analysis of the silicon content of chilled metal was performed at the Division of Metallurgy, The Norwegian Institute of Technology. The oxygen analyses have been done at A/S Norsk Jernverk in an Leco-analyser, i.e., fusion in a graphite crucible under inert atmosphere.

---

*) The multi-run weldments were built up of 21 stringer beads in six layers. Each single bead cross section ratio D/(B+D) was in the range of 0.7 to 0.8 under the conditions employed. (D = deposit cross section, B = fused parent plate cross section.)

4. RESULTS AND DISCUSSION

4.1. Carbon oxidation

The results of carbon determination are presented in Fig. 1. As may be seen from the graph, virtually identical values are obtained for chilled metal and multi-run deposits, while the carbon content measured in electrode tip droplets is lower. In strongly oxidizing atmospheres both curves approach a lower limit close to 0.05% C.

It may be concluded that carbon is not oxidized in the weld pool, which is not present in deposition onto the copper wheel. Carbon must have been lost in one or both of the preceding stages, i.e., at the electrode tip or during the flight through the arc plasma. It seems probable that little if any reaction occurs in the arc plasma, since tip droplet losses alone are more than sufficient to account for the observed total loss.

The excessive loss of carbon from the tip, beyond that recorded in chilled or multi-run weld metal, arises in a process of secondary oxidation after extinction of the arc. This conclusion is supported by the presence of a heavy surface oxide layer on the electrode tip. Metallographic examination of the collected tips (Section 4.6) shows that this subsequent oxidation occurs in the liquid state, leading to the formation of iron-rich multiphase slag within the metal as well as on the droplet surface.

The lack of reaction in the weld pool is further supported by analytical data from Table B.2 (Appendix B), showing the effects of deposition on multi-run welds into which capsules of additions had been implanted. Addition of carbon does not affect the content of other elements beyond a slight reduction of oxygen: 0.003% O in CO_2-shielded welding and 0.030% O when welding under Ar + 20% O_2. In the latter case the manganese content was also reduced by 0.040% Mn, which accounts for part of the loss of oxygen.

Since carbon is seen to oxidize readily at the electrode tip but not at later stages, the supply of oxygen and/or the conditions of nucleation must be more favourable in the former case. It would seem reasonable to assume a high local concentrat on of dissolved oxygen in the hot layers facing the arc. Reaction with carbon in the presence of silicon and manganese would be possible at such surface positions, since these elements are not effective deoxidizers above 1700-1800°C.

The only possible site for CO formation would be the metal/atmosphere interface, homogeneous nucleation of CO bubbles within the liquid metal being a rather unlikely event.

Alternatively, precipitation of slag particles could take place at the lower temperatures prevailing in the bulk of the droplet. The average tip droplet temperature has been estimated by Halmøy /5/ to be only slightly higher than the melting point, and hence such particles could be solid and therefore effective nuclei for bubble formation. Oxidation of carbon may thus start in zones depleted with respect to Si and Mn. Evidence in support of this mechanism has been presented by Corderoy et al /6/, who were able to show depleted zones containing slag particles. Precipitated micro-slag has also been observed in the present work (Section 4.6); however, the time of their formation is not known.

It is probable that oxidation of carbon at the electrode tip proceeds simultaneously along various paths, because the steep temperature gradients and the vigorous convection currents within the droplet will lead to a wide spectrum of conditions. Leaving the question of nucleation sites open, the main features of carbon oxidation in tip droplets may be summarized as follows:

- Continuous absorption of oxygen from the shielding gas into the hot outer layer of the tip droplet.

- Reaction of dissolved oxygen with silicon and manganese to form slag in the cooler parts of the droplet. Convection currents will supply fresh electrode material to the surface. Carbon may be oxidized at this position in the presence of silicon and manganese due to the high temperature, the interface metal/atmosphere serving as a nucleation site.

- Some silicon and manganese, and even iron in the case of high oxygen contents in the gas, may be oxidized at the surface.

- At some distance from the surface silicon and manganese will precipitate as slag, leaving carbon unprotected from oxidation.

- With increased oxygen pick-up, the transport of silicon and manganese becomes insufficient to prevent depletion in regions near the surface. Carbon will now be in control of the oxygen level, and CO bubbles form on precipitated particles. In the case of sufficient supply of carbon from the melting wire to the reaction front, the supply of oxygen is assumed to determine the extent of reaction.

In CO_2-shielded welding, Tables B.1 and B.3, show that the carbon content of the wire has dropped by 0.022% C in chilled metal and by 0.027% C in the electrode tip, the latter figure again including secondary oxidation after extinction of the arc. On the other hand, and increase of the carbon content above that of the wire is observed in multi-run deposition. This reaction does not take place at the electrode tip.

During the period spent in the arc plasma, the droplets will be heated to an average temperature of 2400°C according to measurements by Jelmorini et al /7/. As a result of superheating any slag formed during the tip droplet stage will redissolve, thereby replenishing the silicon and manganese lost in that stage. There is thus no possibility for nucleation on dispersed slag particles, and therefore less chance of loss of carbon. Nucleation at the interface metal/atmosphere is still possible, however, evaporation of manganese and iron (to be discussed in the following section) prevents a free access of oxygen from the shielding gas.

In the case of CO_2-shielded welding oxidation of one atom of carbon will give two molecules of CO. Conceivably, this reaction could be reversed:

$$2\ CO\ (g) = \underline{C} + CO_2\ (g) \qquad (1)$$

Thermodynamically, the reaction shifts to the left at increasing temperature as shown in Fig. 2. In the case of a strongly reducing atmosphere ($p_{CO} = 0.99$), the equilibrium carbon content will be approximately 0.17 per cent at 1600°C, decreasing to about 0.012 per cent at 2400°C. Accordingly, for a reported MIG droplet temperature of about 2400°C (Jelmorini et al /7/), this indicates that pick-up of carbon in the arc plasma is not very likely at such high metal temperatures. Even if the surrounding atmosphere is assumed to consist of nearly pure CO, the equilibrium value will be in the lower range of the expected droplet metal carbon content.

From Table B.1 it may be seen that the carbon content is only 0.005 cent lower than the corresponding value for chilled metal. If this difference in carbon content is assumed to be a result of secondary oxidation after arc extinction, it appears to confirm that pick-up of carbon has not occured during droplet transfer in the arc plasma.

It has been shown above that no carbon is lost from the weld pool when welding under Ar + O_2 (Fig. 1). In CO_2-shielded welding, on the contrary, there is an increase of carbon content. It will be shown in the discussion of oxygen pick-up

(Section 4.4) that this reaction is favoured by low temperatures and therefore probably occurs in the cooler parts of the weld pool. It should be mentioned, however, that pick-up of carbon in this circumstance depends on strongly reducing condtitions.

4.2. Silicon oxidation

The main results from the silicon analyses are presented in Fig. 3. It is seen that only a slight loss of silicon is observed when weld metal is deposited onto the water-cooled copper wheel. Since no macroscopic slag phase was formed on the wheel surface, it follows that the silicon losses must be due to formation of some gaseous reaction product. Evaporation losses may be excluded, since silicon has a very low vapour pressure at all relevant temperatures. The only possible gaseous reaction product is therefore silicon monoxide.

It is generally accepted that formation of silicon monoxide takes place when insufficient oxygen is available to form continuous SiO_2 layers on silicon-bearing liquids. This will be the case under reducing conditions, where oxygen pick-up is prevented by the presence of CO gas. The observed trend in Fig. 3 that the loss of silicon in chilled metal increases with increasing oxygen content in the shielding gas, is believed to be a result of a more extensive CO gas evolution at the electrode tip, according to the reaction:

$$SiO_2 \text{ (in slag)} + CO \text{ (g)} = SiO \text{ (g)} + CO_2 \text{ (g)} \qquad (2)$$

Consequently, the silicon losses are considered to be proportional to the partial pressure of CO gas at the slag/metal interface. The equilibrium partial pressure of SiO as a function of p_{CO} at 1900K (1623°C) and 1996K (1723°C - melting point of pure silica) is shown graphically in Fig. 4. Stoichiometric amounts of CO_2 have been assumed to form in order to calculate p_{SiO}. Since the silicon monoxide partial pressure only shows a minor dependence on temperature, the main factor appears to be the partial pressure of CO. Thus at 1900K, p_{SiO} decreases from about $1.8\ 10^{-3}$ to $1.8\ 10^{-6}$ atm when p_{CO} is reduced from 1 to 10^{-6} atm.

If p_{SiO} and p_{CO} are taken proportional to the observed silicon and carbon losses respectively, a correlation between the loss of silicon and carbon in chilled metal is to be expected. It appears from Fig. 5 that a reasonable correlation exists in this case. The silicon losses are found to be directly proportional to the corresponding carbon losses up to about 40 per cent of the electrode wire C-content. At higher values, deviation from a straight line dependence is seen, indicating that the assumption of proportionality between loss of Si and partial

pressure is no longer valid. The fact the presence of CO gas is the controlling factor appears to be confirmed by the results obtained from weld metal deposition in CO_2. Here the loss of silicon which can be reasonably correlated to SiO formation is considerably higher. About 20 per cent reduction in the chilled metal Si content has been observed. This result is believed to be caused by a higher partial pressure of CO when welding is performed under CO_2. Similar observations have been made by Heile and Hill /8/ by analysis of collected fume in MIG welding. The silicon content in emitted fume was found to increase substantially when CO_2 was present in the shielding gas. Although their thermodynamical interpretation is open to criticism, the experimental data presented are in good agreement with what has been outlined above.

The analyses of multi-run weldments in Fig. 3 show that Si losses mainly take place in the weld pool. As expected, the silicon oxidation increases with increasing oxygen potential in the shielding gas. Thus at 20 vol% O_2 in Ar, the silicon removed from the weld pool by reaction with oxygen amounts to about 0.45 per cent Si. Silicon deoxidation reactions are separately discussed in Section 4.5. Only some comments on the reaction pattern of silicon at the different stages of the process will be given here.

At the temperatures where liquid steel is normally deoxidized, silicon and manganese have a strong affinity to oxygen. Their ability to form stable oxides decreases rapidly with increasing temperature, and above approximately 1800°C, silicon and manganese no longer act as deoxidation agents. Thermodynamically, precipitation of manganese silicate slags are favoured by the lower metal temperatures prevailing at the electrode tip and in the cooler part of the weld pool. At higher temperatures, these oxides become unstable. Consequently, as a result of the metal superheating during droplet transfer through the arc plasma, the macroscopic slag phase formed on the electrode tip surface will re-dissolve in the metal. On slow cooling down to the solidification temperature, this will lead to spontaneous manganese silicate slag precipitation due to the high degree of supersaturation within the liquid metal. The fact that no slag was detected on the chilled metal solid strip surface, confirms the incapability of silicon and manganese to react with oxygen at the temperatures in the arc plasma.

In the case of rapid cooling, the silicon and manganese deoxidation reactions are suppressed. Since precipitation of manganese silicate inclusions are dependent on transport of the reacting elements within the liquid metal, restrictions in supply of reactants will prevent the growth of the oxide nuclei. With decreased oxygen solubility on cooling, this results in spontaneous precipitation of finely-dispersed iron oxide particles within the liquid metal phase. Metallo-

graphic examination of chilled metal has confirmed the presence of a large number of non-metallic inclusions. Electron probe microanalysis indicates that these mainly consist of iron oxide. All particles examined were found to be in the sub-microscopic range, i.e., of a radius below 1 micron.

Apparently, these results are not in agreement with observations made by Corderoy et al /6/*). From examination of collected falling droplets, they concluded that precipitation of manganese silicate slags also occured during metal transfer through the arc plasma. However, since the droplets in this case have not been subjected to a rapid solidification, the observed slag formation is probably more a result of precipitation on cooling than of oxidation at high temperature. This interpretation seems also to be confirmed by the fact that the reported silicon and manganese losses which can be assigned to slag formation are in reasonable agreement with what would be expected from the measured chilled metal oxygen content in Table B.1.

4.3. Vaporization and oxidation of manganese

The results from the manganese analyses of chilled and multi-run weld metal are presented graphically in Fig. 6. It is seen that manganese losses in chilled metal are independent of the oxygen content in shielding gas. This indicates that the losses are more likely a result of the evaporation rather than of oxidation. The vapour pressure of manganese in equilibrium with a melt containing 1.27 per cent Mn, corresponding to the fully-drawn horizontal line in Fig. 6, is shown in Fig. 7. Since the vapour pressure increases strongly with temperature, it is believed that the observed losses are mainly a result of evaporation in the arc plasma. Here the liquid metal temperature reaches its maximum. If the reported droplet temperature of approximately 2400°C is accepted as representative of the actual arc metal temperature, the manganese loss in Fig. 6 corresponds to an equilibrium vapour pressure of about $4.8\ 10^{-2}$ atm. The fact that the Mn losses in chilled metal appears to be independent of shielding gas composition, is further confirmed by the results obtained in CO_2 welding. Identical values for the manganese loss are observed in both cases. Consequently it seems likely that the MIG-CO_2 droplet temperature is approximately of the same level as for Ar-O_2 mixtures.

Similar to silicon, oxidation of manganese is favoured by the lower temperatures prevailing in the cooler part of the weld pool. Here manganese will react with

*) Welding was performed in Ar-O_2 mixtures containing up to 20 per cent oxygen under nearly identical welding conditions.

dissolved oxygen to form slags containing large amounts of MnO. The curve in Fig. 6 for multi-run weld metal deposit indicates that a substantial part of the observed manganese loss occurs in the weld pool, in particular at high oxygen potentials in the shielding gas. Thus at 20 vol% oxygen in argon, the amount of manganese removed from the bath is nearly 0.64 per cent. This corresponds to about 70 per cent of the total manganese loss in welding. A more detailed discussion of the manganese deoxidation reactions taking place during the cooling stage will be given in Section 4.5.

4.4. Pick-up of oxygen

In Fig. 8 the oxygen content of chilled and multi-run weld metal is shown as a function of vol% O_2 in Ar. Some corrections of the chilled metal oxygen analyses have been made before presentation in order to account for the presence of surface oxide films. Consequently, the observed difference in oxygen content of chilled metal deposited in pure argon and electrode wire (equal to 0.033 per cent O) has been subtracted in the plot from the analytical chilled metal values given in Table B.1 (Appendix B). Although the metal was carefully cleaned prior to oxygen determination, local spots of oxide contamination are believed to be a considerable source of error, taking into account the large exposed surface area compared with the total mass of chilled metal (25 to 50 cm^2/g). Normally, the surface to mass ratio will be of the order of 1.5 g/cm^2 *), which in this case would have reduced the correction to about 10-20ppm.

As it appears from Fig. 8, a moderate increase in chilled metal oxygen content is observed up to 15 per cent oxygen in the shielding gas. At higher oxygen levels, a substantial increase in oxygen pick-up can be seen, i.e., an increase of 110 per cent on moving from 15 to 20 vol% O_2 in Ar. The measured values are, however, much too low to account for the silicon and manganese losses in welding. This indicates that considerable amounts of oxygen are absorbed in the hot spot of the weld pool. Calculation of total oxygen consumption may be done on the basis of the observed difference between silicon and manganese content of chilled and multi-run weld metal. Corrections for the oxygen removed from the bath as a result of iron oxide formation can be made if the macroscopic slag composition is known. This lead to the following expression:

$$[\%O]_{total} = [\%O]_{meas.} + \frac{32.0}{28.1}\Delta[\%Si] + \frac{16.0}{54.9}\Delta[\%Mn] + \frac{m}{100}\frac{16.0}{55.8}(\%Fe) \qquad (3)$$

*) The given value corresponds to a cube of 1 g

Here $[\%O]_{meas.}$ is the analytical oxygen content of multi-weldment, $\Delta[\%Si]$ and $\Delta[\%Mn]$ are the observed difference between Si and Mn content of chilled and multi-run weld metal respectively, m is total weight of slag per 100g of weld metal calculated from a mass balance for Si and Mn, and (%Fe) is the analytical iron content in the macro-slag.

The calculated total oxygen absorption on welding is presented graphically in Fig. 9. For 2 and 5 vol% O_2 in Ar, the last member in equation (3) has been ignored due to the lack of information on slag composition. This is not considered to affect the calculated values.

It may be inferred from Fig. 9 that the main oxygen pick-up takes place in the weld pool. Up to about 15 vol% O_2, the total oxygen consumption is a linear function of the O_2-content in the shielding gas, but levels off as the oxygen potential is increased beyond this value. The oxygen content of chilled metal amounts here to only 15-30 per cent of total oxygen absorbed.

In general, pick-up of oxygen from the surrounding atmosphere would be expected to be favoured by the high metal temperature and the large gas/metal interfacial contact area prevailing during droplet transfer through the arc plasma. According to the calculation above, it now appears that pick-up of oxygen at this stage of the process is slaggish. A reasonable explanation of this observed lack of interaction is that the droplets are protected against oxidation by a gaseous layer of argon and/or carbon monoxide close to the metal surface. Further protection against oxidation is supplied by metal vapour, as a result of superheating of the droplets. As a consequence, possible absorption will be slowed down by the diffusion blocking effect of the stagnant gaseous layer. Although the vapour pressure of iron is lower than that of manganese, considerable losses of Fe would be expected due to an activity of Fe close to unity. This is illustrated in Fig. 10 where the equilibrium vapour pressure ratio, p_{Mn} to p_{Fe} is presented graphically in the temperature range from 1600 to 3200°C for a manganese activity of 0.0127. Accordingly, for a droplet temperature of 2400°C, the ratio p_{Mn} to p_{Fe} is closely equal to unity. Analyses of collected fume in MIG welding reported by Heile and Hill /8/ show that the iron losses in welding are substantially higher than that derived from metal composition and published vapour pressures, taking the rates of loss proportional to the vapour pressure. From their experimental data a reasonable estimate of the mass ratio Mn to Fe under the conditions employed will be approximately 1/8. Thus to the loss of manganese observed in the present work about 8 times this amount is expected for the loss of iron, corresponding to a total evapoartion rate of Mn and Fe of about 0.67g per min (or alternatively,

2.25g per 100g deposit). If these elements are considered to be oxidized immediately above the droplet surface to MnO and FeO, respectively, this represents roughly 0.65 per cent of oxygen which could otherwise possibly have been dissolved in the metal.

In the hot spot of the weld pool beneath the arc, the high-velocity plasma jet is likely to sweep away any metal vapour formed and maintain a steady supply of oxygen. Although the gas/metal interfacial contact area available for reaction is much smaller than that of the falling droplets, the strong turbulence existing in the hot part of the pool creates an effective stirring of the liquid metal. Moreover, pick-up of oxygen at this stage is favoured by the increased time available for reaction. If the length of the weld pool hot zone is considered to be roughly 3mm, the time for exposure to the oxidizing gas is of the order of one second. For comparison, the velocity of falling droplets in the MIG arc plasma is reported by Halmøy /9/ to be ablout 2000mm/s, which for a normal flight distance of 10mm will correspond to a reaction time of only 5msec.

The observed trend in Fig. 9 where the total oxygen consumption in welding levels off as the oxygen potential in the shielding gas increases beyond 15 vol% O_2, reflects the fact that at this stage the silicon, manganese and oxygen contents in multi-run weldments approach constant values (Figs. 3,6 and 8). At the same time, the iron content in the slag precipitated on the bead surface increases strongly, from about 12.8 to 27.6 per cent when moving from 15 to 20 vol% O_2 in the shielding gas. It is believed that this course of events is the result of the oxygen solubility being exceeded in the hot part of the weld pool, where excess oxygen reacts to form iron oxide. The oxygen solubility in pure iron up to 1960°C was determined by Distin, Whiteway and Masson /10/, using a levitation technique. Their findings showed that the solubility at high temperatures coincided with extrapolated values from earlier work by Taylor and Chipman /11/. If the upper limit for oxygen solubility in Fig. 9 is taken to be approximately 0.95 per cent, this corresponds to an average hot zone bath temperature of about 2000°C. More recent work by Fischer and Schumacher /12/ indicates that the solubility is higher, corresponding to an average bath temperature of about 1900°C. It may consequently be concluded that the effective bath temperature is between 1900 and 2000°C in the high temperature stage.

At temperatures which apparently are reached in the hot part of the weld pool, the oxygen content in equilibrium with silicon and manganese will be below the solubility limit. For a temperature of 2000°C and a silica activity equal to

unity (relative to pure liquid SiO_2) the oxygen content in equilibrium with 0.5 per cent Si is about 0.2 per cent O. Consequently, silicon would be expected to be in control of the oxygen content, and thus preventing the oxygen concentration to exceed this limit. However, at the existing temperatures there will be no solid/liquid interface present for nucleation of oxide particles, and hence, homogeneous nucleation is the only possibility. According to Sigworth and Elliott /13/, the supersaturation ratio required for homogeneous nucleation of silica is about 80, which indicates that precipitation of silicates is highly unfavourable in the hot part of the weld pool. Upon cooling, however, the supersaturation ratio quickly increases and will exceed the critical value at temperatures below about 1700°C.

For welding in CO_2, the chilled metal oxygen content amounts to nearly 50 per cent of the total calculated oxygen absorption. The oxygen pick-up in chilled metal is nearly identical to that observed for Ar-20 vol% O_2. This is in agreement with statements by Corderoy et al /6/ who claim that a mixture of 15 - 20 vol% O_2 in argon seems to be equivalent to the shielding effect of pure CO_2 with respect to Si and Mn losses in collected tips as well as falling droplets. On the other hand, pick-up of oxygen in the hot part of the weld pool is much lower than would be expected from the chilled metal analysis, as shown by the data for multi-run deposition. The calculated total oxygen consumption of 0.384 per cent O amounts to only 5 to 10 vol% O_2 in argon. It must be concluded that the absorption of oxygen in the weld pool is retarded. An explanation of such a lack of interaction is that the metal in the weld pool is also protected by a gas layer of nearly pure carbon monoxide. In this case the CO_2 in contact with the liquid metal will produce an equivalent amount of CO gas, according to the reaction:

$$CO_2(g) = \underline{O} + CO(g) \qquad (4)$$

Here a massive CO gas evolution from the metal surface will contribute to maintain a protective gas layer of carbon monoxide, limiting the absorption of oxygen. This also offers an explanation to the fact that carbon is subsequently picked up in the weld pool (Section 4.1). Since carbon and oxygen are prevented to react during droplet transfer as well as in the weld pool, a separate pick-up of C and O according to reactions (1) and (4) is possible (pp. 8 and 15, respectively). In Fig. 11 the carbon and oxygen contents in equilibrium with a gas atmosphere of 99 per cent CO and 1 per cent CO_2 are shown graphically as function of temperature. As is indicated in the graph, pick-up of oxygen during droplet transfer in the arc plasma will be favoured by a high metal temperature. At this stage pick-up of carbon is not thermodynamically possible. At the lower

temperatures prevailing in the weld pool, the oxygen pick-up is retarded while that of carbon now will be favoured.

4.5. Deoxidation reactions in the weld pool

Upon cooling in the weld pool from a high temperature a supersaturation with respect to silicon and manganese deoxidation reactions is initially arising. This supersaturation will be released when the conditions leading to oxide precipitation by homogeneous nucleation are reached. From then on, deoxidation will proceed rapidly through growth of nucelei above a critical size. Equilibrium conditions will finally determine the degree of deoxidation to be achieved. In the case of manganese silicates, the separation rate of the dispersed particles is dependent upon their chances to collide and coagulate into larger particles. If solid deoxidation products are formed, the interfacial tension conditions will be rather decisive for the rate of separation. In both cases stirring of the melt set up by turbulence in the weld pool will speed up the phase separation.

Aspects of silicon-manganese deoxidation in steelmaking are extensively investigated and reported in the literature. However, due to the complex path of inclusion separation, it will be difficult to predict the amount of oxygen remaining as inclusions. This applies in particular to the arc welding process where the time for chemical interaction and phase separation is reduced to seconds. Consequently, it will only be possible to describe the deoxidation reaction pattern in more general terms.

It has been mentioned previously that silicon and manganese are more extensively lost in the cooler part of the weld pool. A relationship between the remaining Si and Mn in the melt, would be expected, controlled by the reaction:

$$\underline{Si} + 2MnO = SiO_2 + 2\ \underline{Mn} \qquad (5)$$

Assuming the activity ratio $(a_{MnO})^2 / a_{SiO_2}$ to be constant and independent of the oxygen potential in the shielding gas, equation (5) transforms to:

$$[\%\ Mn] = \text{const}\ \sqrt{[\%\ Si]} \qquad (6)$$

In Fig. 12 equation (6) is plotted by inserting data from Table B.1. As can be seen, a straight line passing through the origin is representative of the experimental data, which confirms that the Si and Mn content in the melt is balanced by an interaction according to equation (5). In Table B.2 it is further

to be seen that addition of Si to the bath leads to a reaction giving an increased Mn content to the melt. A similar addition of Mn, however, does not cause a change in the Si content. Consequently, silicon seems to be in control of the manganese oxidation.

In the deoxidation of steel with silicon and manganese, their ratio can be chosen in order to make these elements stronger deoxidants than either of them alone. This is illustrated in Fig. 13 where the critical silicon and manganese contents of steel in equilibrium with silica-saturated manganese silicate slags are shown at various temperatures. If, for any particular temperature, the composition of steel lies above the curve, manganese does not participate in the deoxidation reaction but solid silica is formed. In the region below the curve, the deoxidation product will be molten manganese silicates, the composition of which is determined by the ratio $[\%Si]/[\%Mn]^2$ in the metal. Consequently, when manganese is added separately to the weld pool, this will cause formation of unsaturated manganese silicates with lower SiO_2 activity, giving conditions for a more effective deoxidation (Table B.2). On the other hand when silicon is added to the pool, the oxygen content will be dependent on the Si and Mn ratio obtained. Thus for welding performed in Ar + 20 vol% O_2 a decrease in oxygen content is observed, while in the case of CO_2 the oxygen content is slightly raised. It may therefore be concluded that additions of silicon will not always result in a more extensive deoxidation, since the lowest possible residual oxygen content is a function of the SiO_2 and MnO activities in the deoxidation product. The apparent decrease in carbon content observed in Table B.2 when extraneous silicon is added, is most probably something which can be assigned to analytical uncertainty.

It is evident from Table B.1 that the oxygen content of weld metal by far exceeds what is to be expected if equilibrium conditions were prevailing down to low temperatures. This is probably not due to a large deviation from chemical equilibrium, but rather a result of incomplete inclusion separation. According to Turkdogan /14/ the time required for precipitated oxides to escape amounts to 5-10 min under laboratory conditions with intensively stirred melts. Since time available in welding is a matter of seconds, incomplete inclusion separation seems to offer a reasonable explanation of the excessive oxygen content. With reference to equilibrium deoxdiation conditions, any straight-forward correlation between silicon, manganese and oxygen in weld metal cannot be expected.

4.6. Metallographic examination of collected electrode tips

Collected electrode tips have been subjected to both optical and scanning electron microscope examination. The results obtained are shown in Appendix C. As it appears from these photographs, surface slags containing large amounts of iron oxide are formed both at high and low oxygen potentials. In the case of a high oxygen content in the shielding gas, the slags have a duplex structure consisting of primary crystals of mangano-wüstite in a matrix of iron-manganese silicate (Fig. C.1 and C.2). As a result of a higher melting point of the FeO-MnO phase, a crust of pure mangano-wüstite forms on solidification. Some porosity in the slag phase is also seen, most probably arising from CO-evolution taking place at the slag/metal interface. Moreover, some of the slag inclusions precipitated within the droplets exhibit a duplex structure composed of solid silica particles in a matrix of iron-manganese silicate (Fig. C.1; large inclusion in upper photograph).

In the metal phase close to the slag layer, it may be observed a zone where Si and Mn are depleted. (electron image of silicon and manganese in Fig. C.3 and C.4). This is taken as a sign of insufficient transport of Si and Mn to the tip surface layers of liquid metal, leaving iron (and carbon) unprotected to extensive oxidation.

5. CONCLUSIONS

The experimental technique applied, melt spinning for rapid solidification, has proved useful to clarify the sequence of reactions occuring in MIG welding by revealing details about oxidation of falling droplets during their passage through the arc plasma. From chemical analysis and metallographic examination of chilled metal deposits, the speed of quenching attained is found to be sufficient to freeze the metal composition established in the arc plasma at high temperature. By analytical comparison of collected electrode tip droplets and multi-run weldments, taking the oxygen content in the shielding gas as the only variable, the reaction pattern in MIG welding can be suggested as follows:

Electrode tip

At the electrode tip silicon, manganese and iron are oxidized, forming surface slags. With increased oxygen absorption, the outer surface metal region becomes depleted with respect to Si and Mn due to inadequate transport of these elements from the bulk of the metal. This in turn leaves

carbon unprotected from oxidation. As a result of the CO evolution, some silicon is lost by SiO gas formation.

Arc plasma

During the droplet transfer in the arc plasma, the previously formed surface slag will dissolve due to metal superheating. Further pick-up of oxygen is to a large extent slowed down because of the shielding effect of manganese and iron evaporation. The falling droplets leaving the arc plasma zone are characterized by a farly high supersaturation with respect to the carbon-oxygen reaction.

Weld pool - hot part

In the hot part of the weld pool immediately beneath the arc, oxygen is extensively dissolved in the melt. Referred to the welding parameters applied and with 20 vol% O_2 in argon, it appears that the oxygen pick-up occurs to an extent corresponding to the solubility at about 1900 to 2000°C. The reason for this is that Si and Mn at relevant concentrations are inable to participate in deoxidation at this of temperature. The carbon deoxidation on the other hand, is blocked by the absence of nucleation possibilities.

When CO_2 is used as a shielding gas, the oxygen absorption in the hottest part of the pool is more restricted, probably as a result of carbon dioxide decompositon at the metal surface leading to formation of a protecting CO gas layer. This also offers a reasonable explanation of the fact that the carbon content in the weld pool increases relative to be tip droplets.

Weld pool - cooling stage

Upon cooling of the metal in the weld pool down to the solidification temperature, silicon and manganese will react with dissolved oxygen and precipitate as micro-slag particles. This deoxidation reaction will be initiated by a homogeneous nucleation from a supersaturated melt, and from there on proceed rapidly towards equilibrium. However, the conditions for micro-slag separation will be highly unfavourable, leading to high and rather unpredictable analytical oxygen contents.

Practical application of results is not a primary concern of the present programme, which is intended to supply fundamental information on the physics and chemistry of the process. Perhaps the most surprising feature of the (Ar + O_2)-shielded process is the enormous flux of dissolved oxygen introduced in the hot part of the pool and rejected during cooling. The limit of oxygen absorption is probably not controlled by the oxygen content of the gas alone, but by the oxygen solubility in liquid iron (or in liquid steel, which amounts to the same at temperature close to 2000°C). The alloy content of the solidified weld metal (about 0.3% Si and 0.6% Mn) is thus as much a result of weld pool temperatures as of the amounts of Si, Mn and O charged into the process, because liquid iron would be oxidized in preference of Si and Mn at a lower alloy content. On this basis it would not be surprising to find that successful welding could be performed even at higher oxygen contents in the shielding gas than 20% O_2.

Trondheim, August 20th 1982

Øystein Grong

Øystein Grong

341094 ØG/åh
D:ARB5

6. REFERENCES

1. Maringer, R.E.:
Battelle's Columbus Laboratories (U.S.)

2. Guile, A.E., Hitchcock, A.H.:
Time variation in copper cathode erosion rate for long-duration arcs.
J. Phys. D: Appl. Phys., Vol. 8 (1975), p. 427-433

3. Hitchcock, A.H., Guile, A.E.:
Erosion of copper cathodes by moving arcs at currents of 45 - 800 A.
PROC. IEE, Vol. 122 (1975), No. 7, p. 763-764.

4. Huang, S.C., Fiedler, H.C.:
Effect of wheel surface conditions on the casing of amorphous metal ribbons.
Met. Trans.- Vol. 12A (1981), p. 1107-1112

5. Halmøy, E.:
Wire feed rate, droplet temperature and effective anode melting potential.
Int. Conf. Arc Physics and Weld Pool Behaviour, London 8-10 May 1979, p.49-57. Publ. The Welding Institute.

6. Corderoy, D.J.H., Wills, B., Wallwork, G.R.:
Gas/metal reactions in MIG arc plasma.
Int. Conf. Weld Pool Chemistry and Metallurgy, London 15-17 April 1980, p. 147-153. Publ. The Welding Institute.

7. Jelmorini, G., Tichelaar, G.W., Van den Heuvel, G.J.P.M.:
Droplet temperature measurements in arc welding.
IIW Doc. 212-411-77.

8. Heile, R.F., Hill, D.C.:
Particulate fume generation in arc welding.
Weld. Jn., Vol. 54 (1975), Res. Suppl., p. 201s-210s.

9. Halmøy, E.:
A study of pulsed drop formation in MIG welding arcs.
Department of Electron Physics, Royal Institute of Technology
S-100 44 Stockholm 70, Sweden (June 1973).

10. Distin, P.A., Whiteway, S.G., Masson, C.R.:
Solubility of oxygen in liquid iron from 1785 to 1960°C. A new technique for the study of slag-metal equilibria.
Canad. Met. Quart., Vol. 10 (1970) No. 1, p. 13-18.

11. Taylor, C.R., Chipman, J.:
Trans. AIME 154: 228 (1943)

12. Fischer, W.A., Schumacher, J.F.:
The solubility of oxygen in pure iron from melting point to 2046°C, determined using the levitation melting method.
Arch. Eisenhüttenwes., Vol. 49 (1978), No. 9, p. 431-435.

13. Sigworth, G.K., Elliott, J.F.:
The conditions for nucleation of oxides during the silicon deoxidation of steel., Met. Trans., Vol. 4 (1973), p. 105-113

14. Turkdogan, E.T.:
Deoxidation of steel; review-paper.
Int. Conf. Chemical Metallurgy of Iron and Steel, University of Sheffield 19-21 July 1971, p. 153-170. Publ. The Iron and Steel Institute, London.

15. Barin, I., Knacke, O.:
The thermochemical properties of inorganic substances.
Springer-Verlag, 1973.

16. JANAF Thermochemical Tables - Second Edition
NSRDS, National Bureau of Standards (U.S.), 1971.

17. Kubaschewski, O., Alcock, C.B.:
Metallurgical Thermochemistry, 5th Edition.
Pergamon Press, 1979.

18. Turkdogan, E.T.:
Deoxidation of steel - What happens from tap to solidification.
Second Operating Metallurgy Conference, Philadelphia, Pennsylvania, 5-8 December 1966. Publication in Journal of Metals.

19. Elliott, J.F., Gleiser, M., Ramakrishna, V.:
Thermochemistry for steelmaking, Vol. II.
Adison - Wesley Publ. Co./Pergamon Press, London 1963.

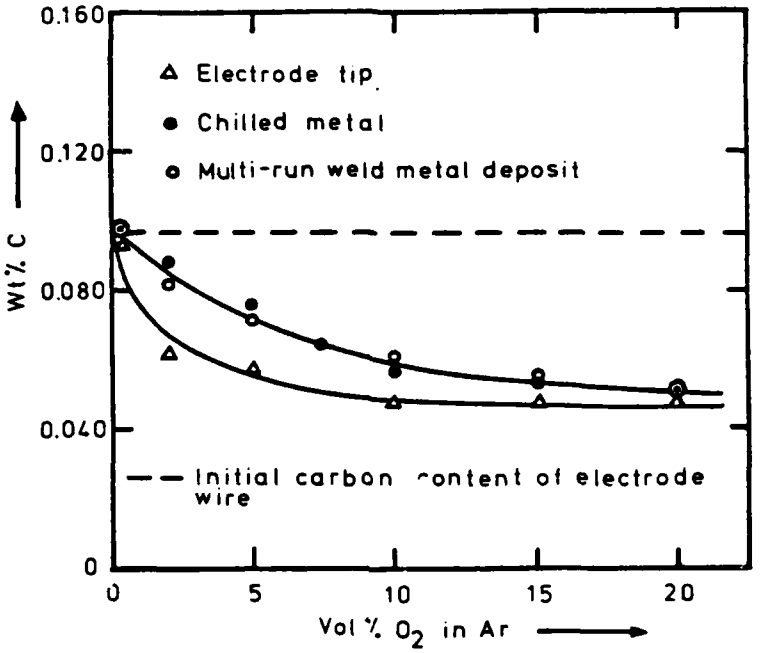

Fig. 1. The carbon content of electrode tip, chilled metal and multi-run weld metal deposit versus the O_2 content in the shielding gas

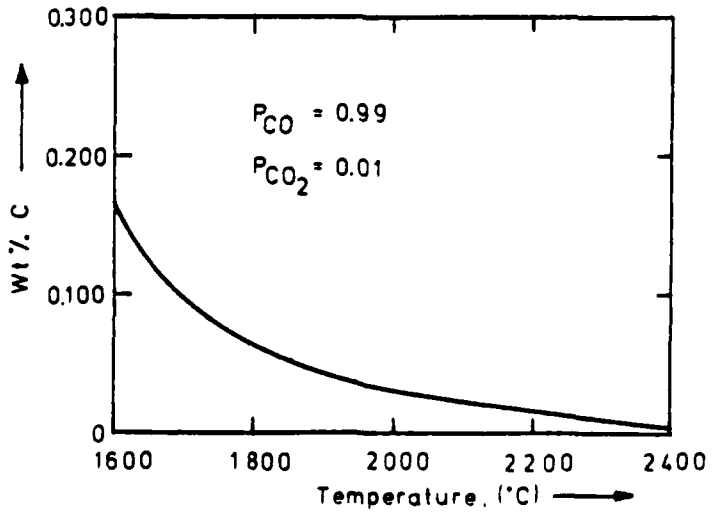

Fig. 2. The equilibrium $2CO(g) = \underline{C} + CO_2(g)$ for $p_{CO} = 0.99$ resp. $p_{CO} = 0.01$ versus temperature. Calculation based on data from /19/

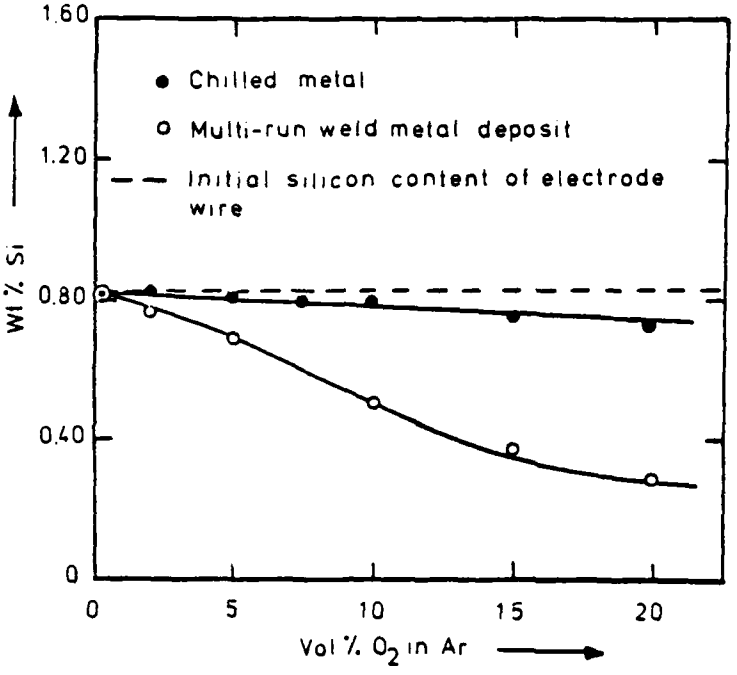

Fig. 3. The silicon content of chilled metal and multi-run weld metal deposit versus the O_2 content in the shielding gas.

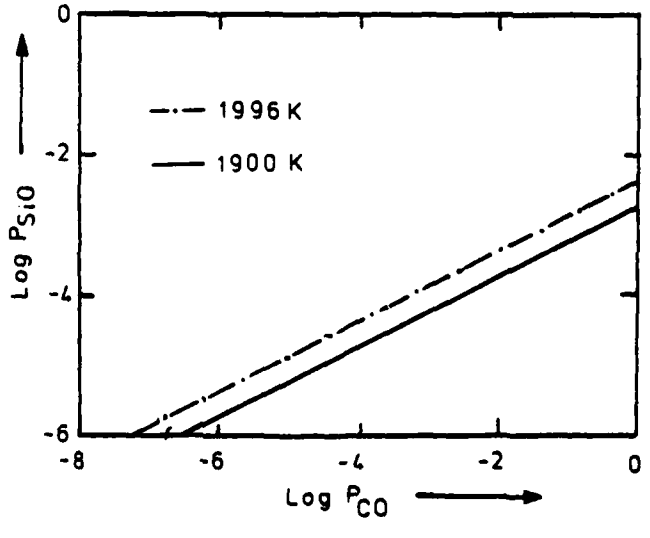

Fig. 4. The equilibrium partial pressure of SiO versus P_{CO} at 1900 and 1996 K. Calculation based on data from /15/ and /16/.

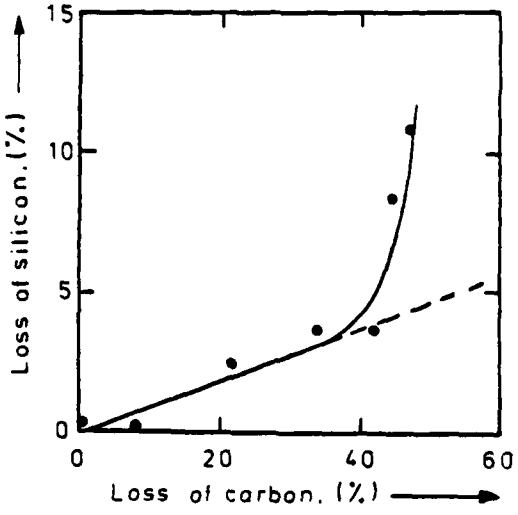

Fig. 5. The correlation between loss of silicon and carbon in chilled metal (per cent of initial Si resp. C content of electrode wire).

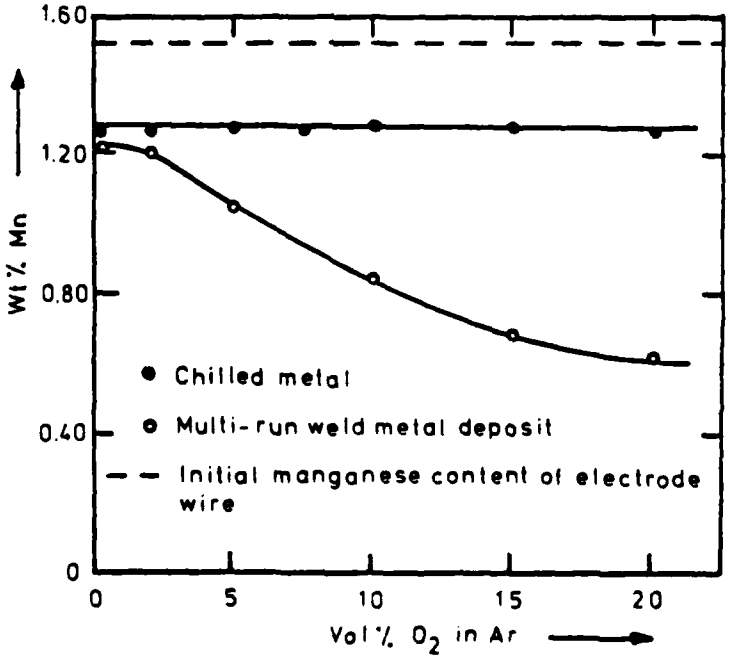

Fig. 6. The manganese content of chilled metal and multi-run weld metal deposit versus of the O_2 content in the shielding gas.

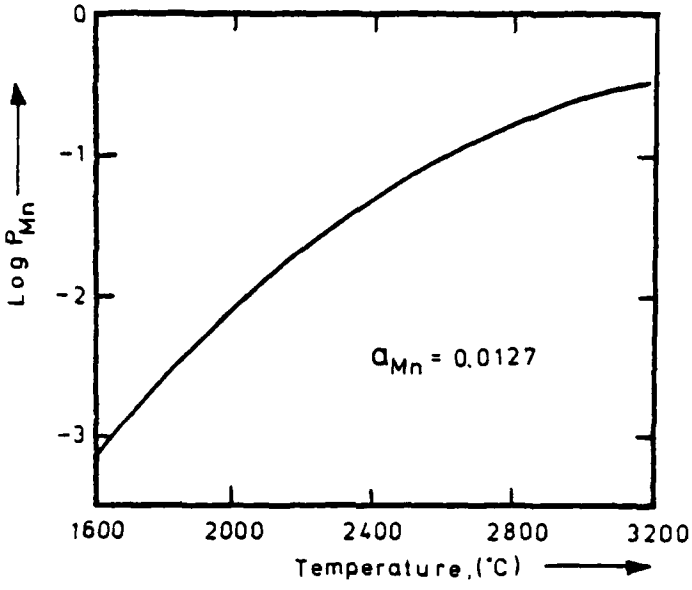

Fig. 7. The vapour pressure of manganese in equilibrium with a melt containing 1.27 per cent Mn versus temperature. Calculation based on data from /17/.

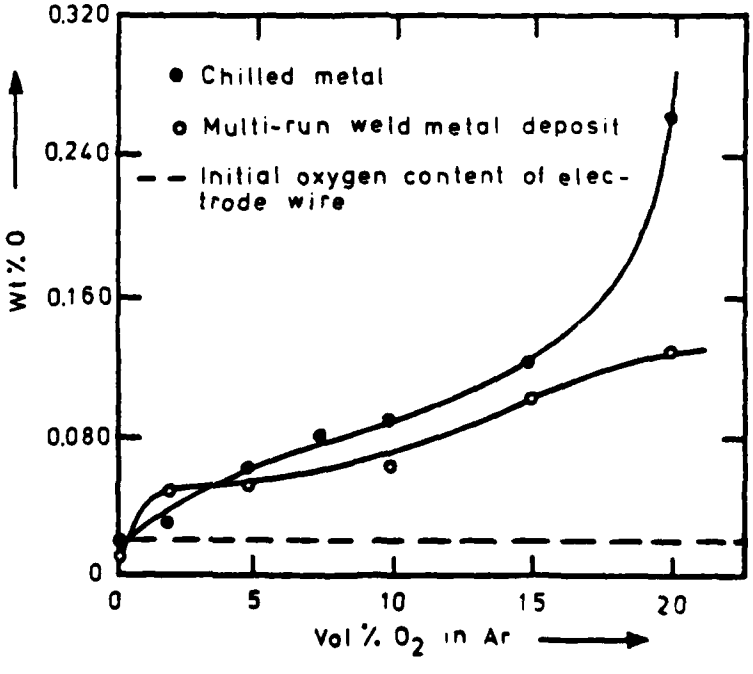

Fig. 8. The oxygen content of chilled metal and multi-run weld metal deposit versus the O_2 content in the shielding gas.

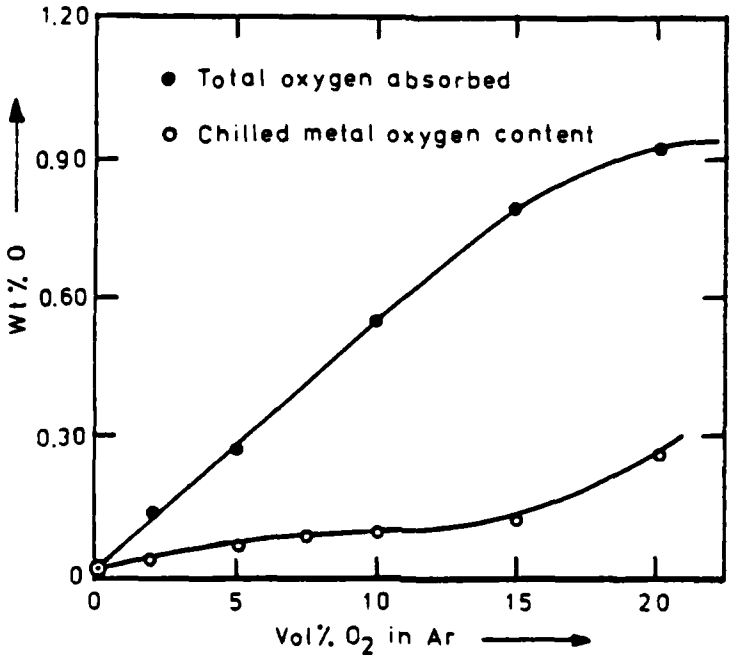

Fig. 9. Observed chilled metal oxygen content and calculated total oxygen absorption

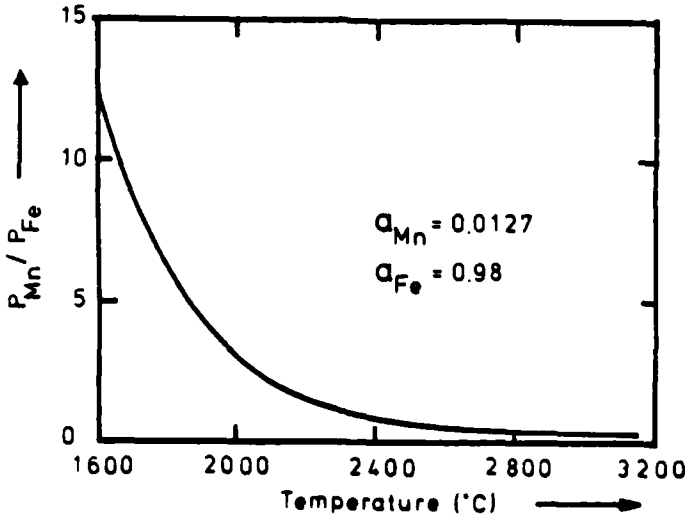

Fig. 10. The equilibrium vapour pressure ratio p_{Mn} to p_{Fe} versus temperature. Calculation based on data from /17/.

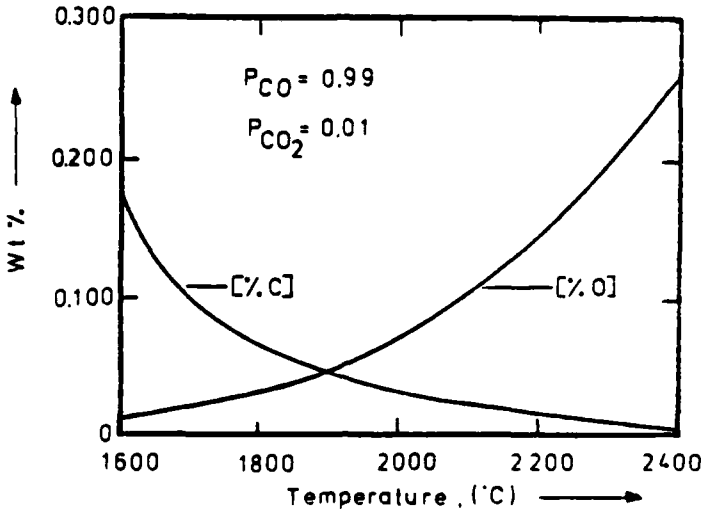

Fig. 11. The equilibrium $2CO(g) = \underline{C} + CO_2(g)$ and $CO_2(g) = \underline{O} + CO(g)$ for $p_{CO} = 0.99$ resp. $p_{CO} = 0.01$ versus temperature. Calculation based on data from /19/.

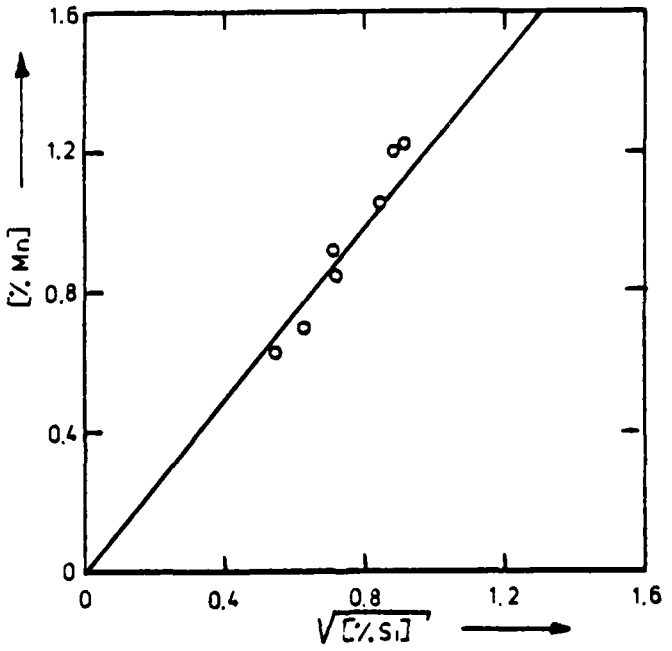

Fig. 12. Correlation between manganese and silicon content in multi-run weld metal deposit.

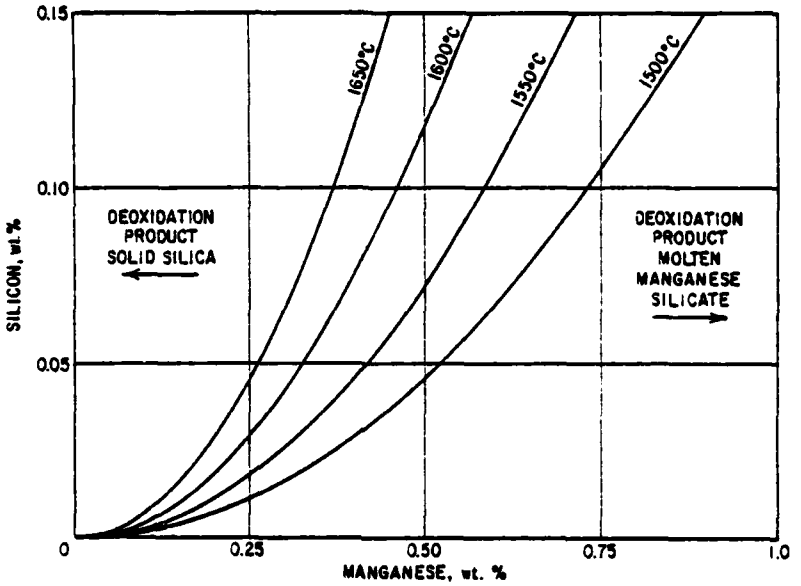

Fig. 13. Critical silicon and manganese contents of iron in equilibrium with silica saturated deoxidation product, almost pure manganese silicate at various temperatures. From /18/.

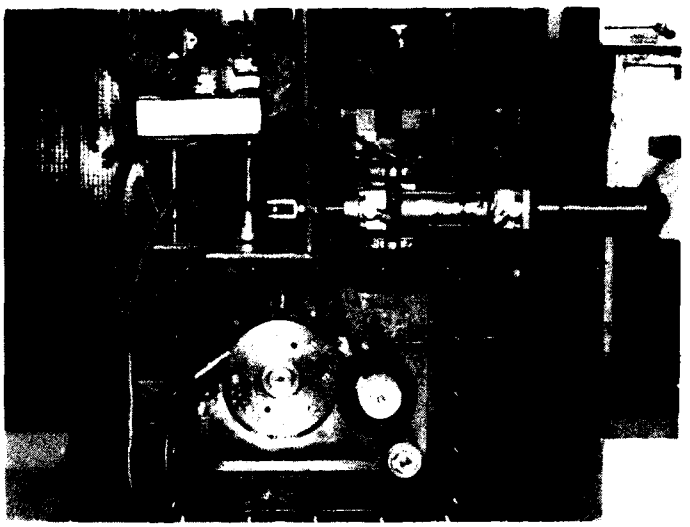

Fig. A.1. Equipment developed for deposition of weld metal against the copper wheel.

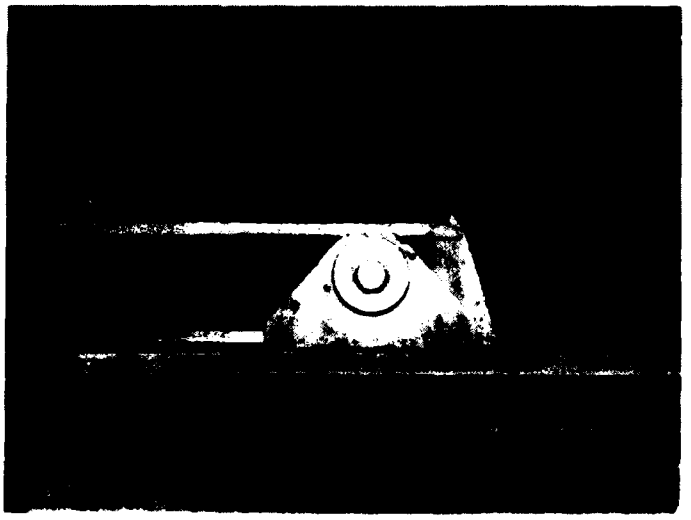

Fig. A.2. Equipment used for multi-run weld metal deposition on plate.

Table B.1. Analysis of electrode tip, chilled metal, multi-run weld metal deposit and slag formed on the bead surface.

Shielding gas		Metal phase				Slag phase		
		Wt%C	Wt%O	Wt%Si	Wt%Mn	Wt%Si	Wt%Mn	Wt%Fe
Pure Ar	Electrode tip	0.096	-	-	-	-	-	-
	Chilled metal	0.097	0.053	0.83	1.26	-	-	-
	Multi-run weld metal deposit	0.098	0.010	0.82	1.22			
Ar+2%O_2	Electrode tip	0.062	-	-	-	-	-	-
	Chilled metal	0.089	0.064	0.83	1.27	-	-	-
	Multi-run weld metal deposit	0.081	0.047	0.77	1.20	-	-	-
Ar+5%O_2	Electrode tip	0.058	-	-	-	-	-	-
	Chilled metal	0.076	0.092	0.81	1.27	-	-	-
	Multi-run weld metal deposit	0.071	0.052	0.70	1.05	-	-	-
Ar+7.5%02	Chilled metal	0.064	0.113	0.80	1.27	-	-	-
Ar+10%O_2	Electrode tip	0.048	-	-	-	-	-	-
	Chilled metal	0.056	0.120	0.80	1.28	-	-	-
	Multi-run weld metal deposit	0.061	0.061	0.51	0.84	20.10	31.61	7.95
Ar+15%O_2	Electrode tip	0.048	-	-	-	-	-	-
	Chilled metal	0.054	0.157	0.76	1.28	-	-	-
	Multi-run weld metal deposit	0.056	0.103	0.38	0.69	18.66	28.37	12.75
Ar+20%O_2	Electrode tip	0.048	-	-	-	-	-	-
	Chilled metal	0.052	0.295	0.74	1.26	-	-	-
	Multi-run weld metal deposit	0.052	0.130	0.29	0.62	18.33[1] 20.94[2]	21.67[1] 27.88[2]	27.58[1] 10.99[2]
Pure CO_2	Electrode tip	0.070	-	-	-	-	-	-
	Chilled metal	0.075	0.221	0.66	1.26	-	-	-
	Multi-run weld metal deposit	0.102	0.078	0.49	0.92	21.09	32.22	4.83

1) Collected bead surface slag

2) Electron probe microanalysis of trapped macroscopic slag in multi-run weldment

Table B.2. Analysis of beads deposited on multi-layer weld metal containing additions of C, Si and Mn implanted in metal. Values in brackets from Table B.1 without additions.

Shielding gas	Implanted element	Weld metal			
		Wt%C	Wt%O	Wt%Si	Wt%Mn
$Ar+20\%O_2$		(0.052)	(0.130)	(0.29)	(0.62)
	Carbon	0.136	0.100	0.28	0.58
	Silicon	0.045	0.109	0.79	0.71
	Manganese	0.054	0.077	0.28	1.31
Pure CO_2		(0.102)	(0.078)	(0.49)	(0.92)
	Carbon	0.185	0.075	0.48	0.92
	Silicon	0.091	0.088	0.84	1.00
	Manganese	0.105	0.071	0.50	1.87

Table B.3. Chemical composition of electrode wire.

Element	% C	% O	% Si	% Mn
OK 12.51	0.097	0.020	0.83	1.52

Light area in surface slag corresponds to an average composition of 4.5% Mn and 66.3% Fe. Only traces of Si were detected.

200X

Dark area in surface slag corresponds to an average composition of 3.3% Mn, 55.8% Fe and 11.0% Si.

500X

Fig. C.1 Surface slag formed on electrode tip droplet in Ar + 15 vol% O_2.

Light area in surface slag corresponds to an average composition of 2.9% Mn and 67.3% Fe. Only traces of Si were detected.

200X

Dark area in surface slag corresponds to an average composition of 3.8% Mn, 48.7% Fe and 11.1% Si.

500X

Fig. C.2. Surface slag formed on electrode tip droplet in Ar + 20 vol% O_2.

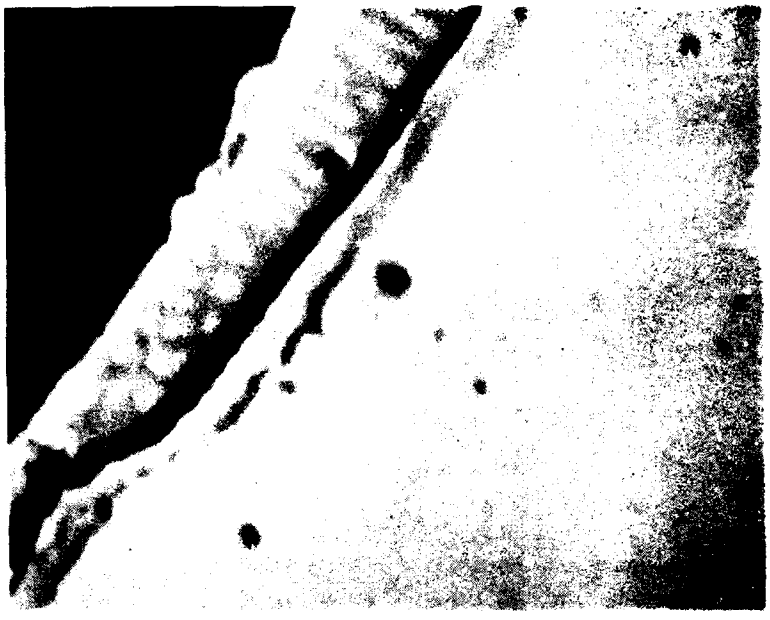

Fig. C.3. Electron image of surface slag formed on electrode tip droplet in Ar + 2 vol% O_2 (2000X).

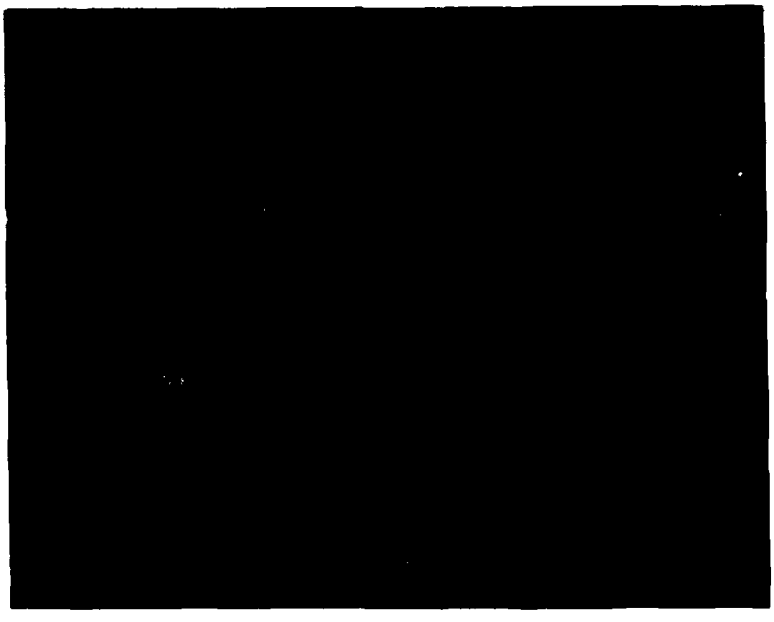

Fig. C.3.1. Eletron image of silicon

Fig. C.3.2. Electron image of magnanese

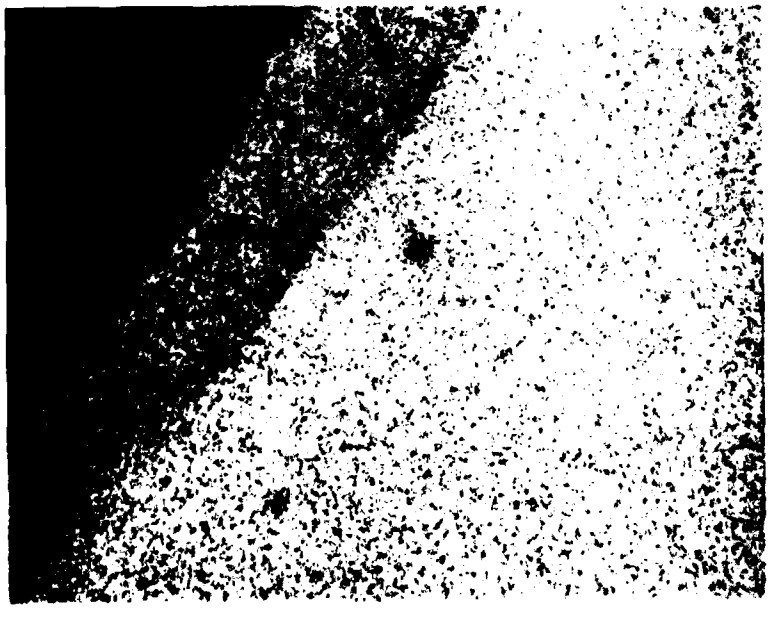

Fig. C.3.3. Electron image of iron.

Fig. C.4. Electron image of surface slag formed on electrode tip droplet in CO_2 (2000X).

Fig. C.4.1. Electron image of silicon

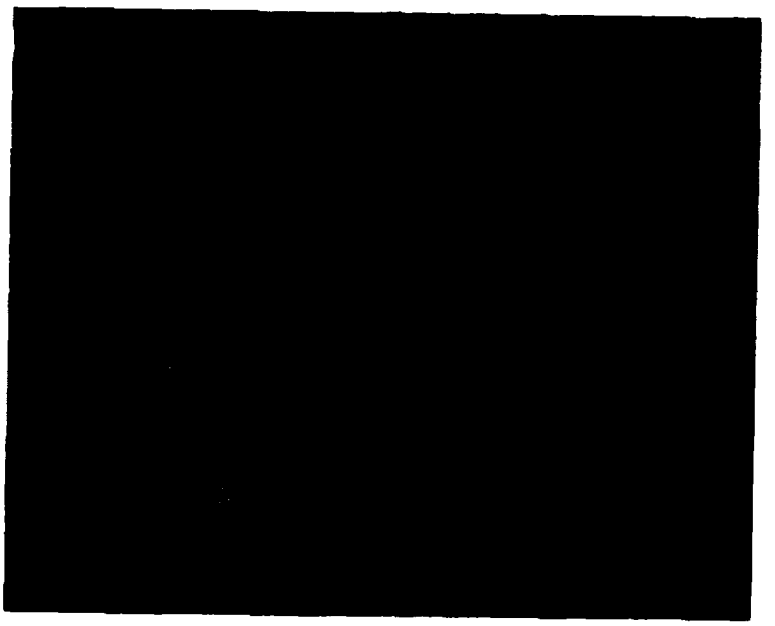

Fig. C.4.2. Electron image of manganese

Fig. C.4.3. Electron image of iron


DATE
ILME